LANDSLIDE IN DOSSENA (BG): COMPARISON BETWEEN INTERFEROMETRIC TECHNIQUES

Daniele Perissin, Riccardo Piantanida, Davide Piccagli, Fabio Rocca

Politecnico di Milano, Via Ponzio 34/5, 20133 Milano, Italy

daniele.perissin@polimi.it

ABSTRACT

In this work the landslide of Dossena (BG, Italy), located in a mountainous area north of Milan, is taken as case study to compare different spaceborne SAR interferometric techniques and find the best answer to the requests of the local geologists. The landslide of Dossena, in fact, is known since almost 20 years and it has been monitored with levelling instruments for some periods. But, due to economical and technical problems, the precise delimitation of the sliding area was not yet known. Spaceborne SAR interferometric techniques are able to detect terrain movements within wide areas and thus represent the ideal instrument to find the borders of such deformations. The most accurate interferometric algorithm at the moment is the Permanent Scatterers (PS) technique, developed by POLIMI. But the PS technique requires that a target, in order to be detected as coherent, shows an electromagnetic stability for the whole time-span of the acquisitions. This is usually the case of targets in urban sites, but not in mountainous areas. In this work we present new hints for multi-temporal analysis of SAR images to extract information also by partially coherent targets and thus provide more spatially dense deformation maps in extra-urban areas. A novel processing chain has been implemented and applied to the Dossena case study, allowing to increase the number of measure points and thus to better identify the borders of the landslide.

INTRODUCTION

Dossena is a small municipality located in a mountainous area in the Italian province of Bergamo. Since 1998 part of the area of Dossena has been classified as risk zone due to an active landslide on its territory. To monitor the ground displacement two inclinometer were installed in two sensible points. However, most of the risk zone is not monitored and, even more critical, the boundary of the risk zone have never been checked with deformation instruments. Thus, local geologists decided to commission the deformation analysis to spaceborne radar techniques in order to get an effective overview of the phenomenon.

To this aim, SAR Interferometry [1] is a remote sensing technique able to recover high-resolution topographic profiles (precision ~10m) and to highlight possible ground deformation phenomena (precision ~10mm). Topography and movement are extracted from interferograms, complex products of two scenes gathered at different times with different looking angles over the same area of interest. The main limitations of InSAR are temporal and geometrical decorrelation, caused by the variation of the ground reflectivity as a function of the acquisition time and incidence angle. Moreover, interferograms are affected by turbulences related to the spatially variant water vapour content in the atmosphere.

The Permanent Scatterers (PS) Technique [2], developed at POLIMI in late nineties, is a powerful tool in the context of InSAR. By looking at radar targets that maintain unchanged their electromagnetic signature during the whole observation span, the PS technique allows to solve the classical problems of interferometry. The technique has been successfully applied to different cases, from ground deformation monitoring [3] to building stability analysis [4], and also to recover digital elevation maps (DEM) [5]. The accuracy achievable by means of the PS technique is in the order of 1m in the estimate of the target height and 1mm in the estimate of the target displacement [6]. The main drawback of the PS approach is the low spatial density of permanent targets, in particular in extra-urban areas. Indeed the lack of measure points can prevent from monitoring with spaceborne SAR techniques an area of interest affected by deformations. In this work we present a new approach that relax the strict conditions imposed by the PS technique in order to extract information also from partially coherent targets and thus to increase the spatial distribution of measure points. In particular, three main modifications have been introduced:

1. the images of the data-set are no more required to interfere with a unique common Master image as in the PS technique;
2. in the estimate of the target height and displacement only the coherent interferograms are evaluated;
3. considering extended targets a spatial filtering is applied to enhance the signal to noise ratio of the interferometric phase.

The new approach was successfully applied to the case study of Dossena and the boundary of the landslide was for the first time measured. In the following we analyse in depth the main steps of the innovative algorithm.

ALGORITHM

Let us denote with s_i the i-th complex SAR image (with $i = 1,...N$). The interferogram between the images i and j can thus be expressed as $I_{i,j} = s_i \cdot s_j*$. Taking the target p_0 as reference point, the interferometric phase of target p $\Delta f^{i,j} = \angle I_{i,j}$ depends on its geometrical location as well as on its displacement, atmospheric disturbances and noise. In particular the terms that depend on the target p height $\Delta h_{p,p_0}$ and linear deformation trend $\Delta v_{p,p_0}$ are expressed respectively by

$$\Delta f_{H,p,p_0}^{i,j} = \frac{4p}{l} \frac{1}{R\sin q} \Delta h_{p,p_0} Bn_{i,j} \quad (1)$$

and

$$\Delta f_{D,p,p_0}^{i,j} = \frac{4p}{l} \Delta v_{p,p_0} Bt_{i,j} \quad (2)$$

where $Bn_{i,j}$ is the interferometric normal baseline, $Bt_{i,j}$ the temporal baseline, l the wavelength, q the looking angle and R the sensor-target distance.

Within the PS technique, the target height and velocity are estimated by maximizing the temporal coherence $\mathbf{x}_p$ [2] (we omit index p_0 to lighten the notation):

$$(\Delta \hat{h}_p, \Delta \hat{v}_p) = \arg\{\max \|\mathbf{x}_p\|\} \quad (3)$$

where

$$\mathbf{x}_p = \frac{\sum_{i=1}^{N} e^{j\left(\Delta f_p^{i,j} - \Delta \overline{f}_{H,p}^{i,j} - \Delta \overline{f}_{D,p}^{i,j}\right)}}{N} \quad (4)$$

In (4) the following term can be highlighted:
- $\Delta f_p^{i,j}$ is the acquired interferometric phase (compensated for the terms that do not depend on elevation and linear deformation trend)
- $\Delta \overline{f}_{H,p}^{i,j}$ is the elevation-dependent term given by (1)
- $\Delta \overline{f}_{D,p}^{i,j}$ is the deformation trend-dependent term given by (2)

In the classical PS analysis the interferometric phase in (4) is generated by referring all images to a common Master acquisition. In the normal baseline – temporal baseline space this configuration can be represented with a star graph as in Figure 1 on the left, where each point indicates an image and each connection an interferogram in the Dossena data-set. In this framework, the graph connection assures the temporal continuity of the deformation measurements and thus the possibility of unwrapping the phase time series. On the other side, the main drawback of this combination is to pretend that each image can coherently interfere with the Master acquisition. Other less restrictive configurations are also possible. E.g. in the SBAS technique [7] only the interferograms with small normal baselines are used in order to reduce the geometrical decorrelation and therefore to easier estimate the deformations. However, in such a way the graph connection is lost and the unwrapping procedure becomes critical. An other approach is standard interferometry, that usually exploits interferograms with small both geometrical and temporal baselines. Interferograms can then be combined with stacking procedures [8]. Here we propose a new methodology to create a set of interferograms from a given data-set. Without imposing any pre-defined decorrelation model, we search for the minimum best coherent graph connecting all the images of the data-set (usually known as the Minimum Spanning Tree, MST). To reach this purpose with a limited computational cost, we assign to each graph connection i,j the absolute value of the spatial coherence $\mathbf{g}_p^{i,j}$ averaged over a set of given points. Then we search among the $N(N-1)/2$ possible interferograms for the MST that
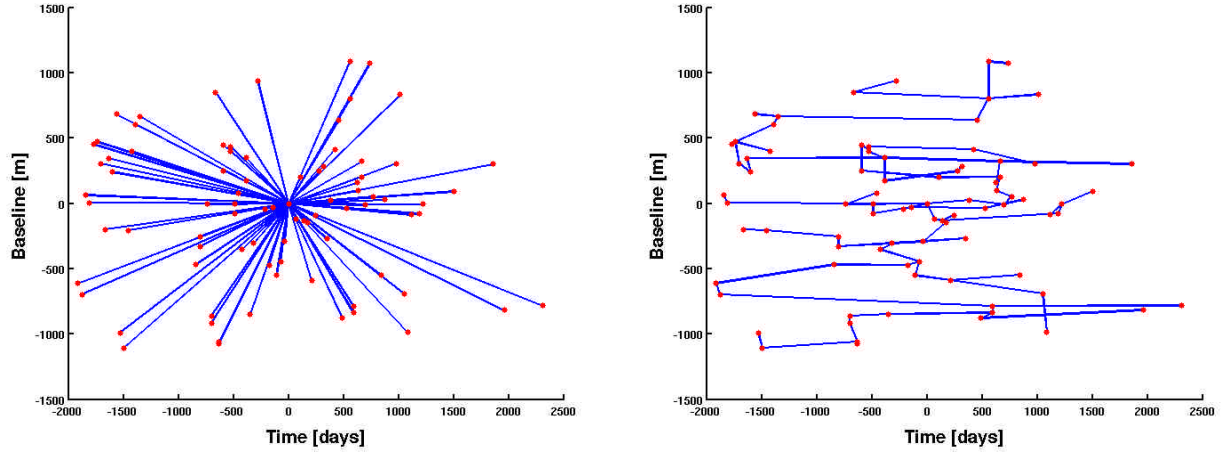
Figure 1 – Comparison between the images graph adopted in the PS technique (on the left) and the MST obtained by maximizing the average coherence (on the right).

maximizes the average coherence. The spatial coherence $\boldsymbol{g}_p^{i,j}$ of point p is retrieved as the normalized cross-correlation coefficient between images i,j over an appropriate neighbourhood $Win(p)$ of p

$$\boldsymbol{g}_p^{i,j} = \frac{\sum_{Win(p)} S_i S_j^*}{\sqrt{\sum_{Win(p)}\left|S_i\right|^2 \sum_{Win(p)}\left|S_j\right|^2}} \quad (5)$$

Figure 1 on the right shows the obtained graph in the Dossena data-set. As visible in the picture, many selected connections have small normal baselines, but not all interferograms follow this rule. Moreover, the graph is connected.
The configuration in Figure 1 on the right is thus on average the minimum best way to combine the available images. However, the set of coherent interferograms that carry information can be different from point to point. Again, only PS's are coherent in all interferograms. Thus, in order to estimate height and deformation trend also of partially coherent targets, we have to choose a subs-set of coherent interferograms for each point. To this purpose we can exploit the absolute value of the spatial coherence $\boldsymbol{g}_p^{i,j}$ of point p. By inserting it as a weight in the estimation process, only coherent interferograms will determine the result. The temporal coherence in (4) becomes then

$$\boldsymbol{x}_p = \frac{\sum_{(i,j)}\left|\boldsymbol{g}_p^{i,j}\right| e^{j\left(\Delta \boldsymbol{f}_p^{i,j} - \Delta \overline{\boldsymbol{f}}_{H,p}^{i,j} - \Delta \overline{\boldsymbol{f}}_{D,p}^{i,j}\right)}}{\sum_{(i,j)}\left|\boldsymbol{g}_p^{i,j}\right|} \quad (6)$$

where the denominator has been modified to normalize the outcome.
Figure 2 brings a graphical representation of the concept with two examples (left and right). The three pictures show the phase residuals (after compensating for the geometrical and the movement terms) of a given point as a function respectively of the spatial coherence (top), the normal (centre) and the temporal (bottom) baselines. The red dots are the phase residuals in the interferograms with spatial coherence > 0.4. What is clearly recognizable from Figure 2 is that assigning a weight to the phase values allows to identify the information and to discard the noise (the dispersion of the phase values decreases with the coherence). From the distribution of red dots as a function of the normal and temporal baselines it can also be noted that the two selected examples are affected more by temporal than by geometrical decorrelation (red dots are concentrated in small temporal baselines). This fact can have consequences on the accuracy of the estimate of the deformation trend. The smaller the lever arm, the less accurate is the estimate. In order to evaluate the accuracy, we introduce the index Bt_p^{eff} for each point p that quantifies the effective set of temporal baselines used in the estimate:
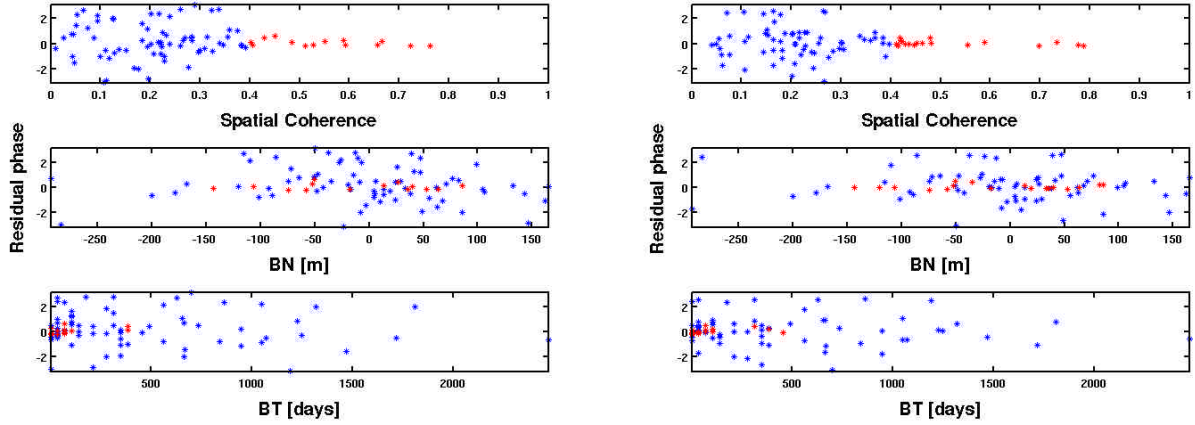
Figure 2 – Two examples (left and right) of residual phase series after removing for the height and deformation trend terms, as a function of spatial coherence (top), normal baseline (centre), temporal coherence (bottom). Red dots: phase samples corresponding to spatial coherence >0.4.

$$Bt_p^{eff} = \frac{\sum_{(i,j)} \left|\boldsymbol{g}_p^{i,j}\right| \cdot \left|Bt^{i,j}\right|}{\sum_{(i,j)} \left|\boldsymbol{g}_p^{i,j}\right|} \qquad (7)$$

Index (7) is the average temporal baseline, weighted by the absolute value of the spatial coherence associated to point p. Figure 3 on the left reports index (7) in Dossena for all the analysed points in a logarithmic scale. The picture shows that most of targets in Dossena has low coherence in MST interferograms with high temporal baselines. In order to increase the effective temporal baseline (7), more connections can be added to the MST. By e.g. doubling the number of graph connections (selecting the most coherent interferograms not yet used) we obtain the graph shown in Figure 4 on the right. The corresponding effective baseline map is reported in Figure 3 on the right. In spite of a limited growth of computational costs, a reasonable expected accuracy is reached.

The last aspect we take into consideration is the possible extended nature of the target at hand. To this aim we apply a spatial filtering to strengthen the estimate of the interferometric phase associated to the target. Thus we introduce in the expression of the temporal coherence of target p (5) the phase of the spatial coherence $\angle \boldsymbol{g}_p^{i,j}$ instead of the phase of the single pixel

$$\boldsymbol{x}_p = \frac{\sum_{(i,j)} \left|\boldsymbol{g}_p^{i,j}\right| e^{j\left(\angle \boldsymbol{g}_p^{i,j} - \Delta \overline{\boldsymbol{F}}_{H,p}^{i,j} - \Delta \overline{\boldsymbol{F}}_{D,p}^{i,j}\right)}}{\sum_{(i,j)} \left|\boldsymbol{g}_p^{i,j}\right|} \qquad (8)$$

Figure 5 shows two examples (left and right) of phase residuals after compensating for the terms dependent on height and linear deformation trend. In the top images the phase is relative to a single pixel, in the bottom images the phase has been obtained by estimating the spatial coherence. Considering extended targets, the averaging process increases the signal to noise ratio.
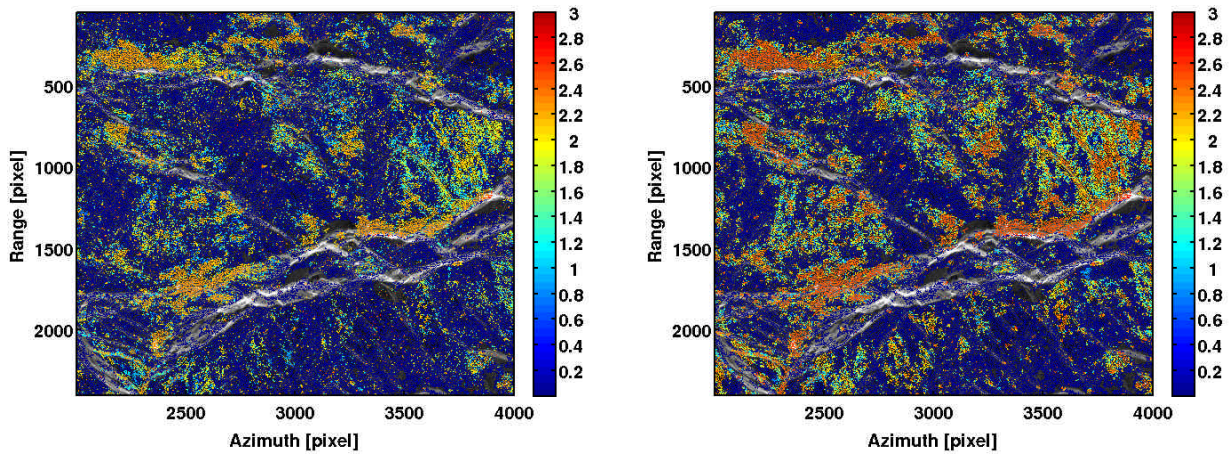
Figure 3 – Effective temporal baseline in Dossena, obtained with the MST (on the left) and by doubling the number of interferograms (on the right). The temporal baseline is shown in a colour log-scale.
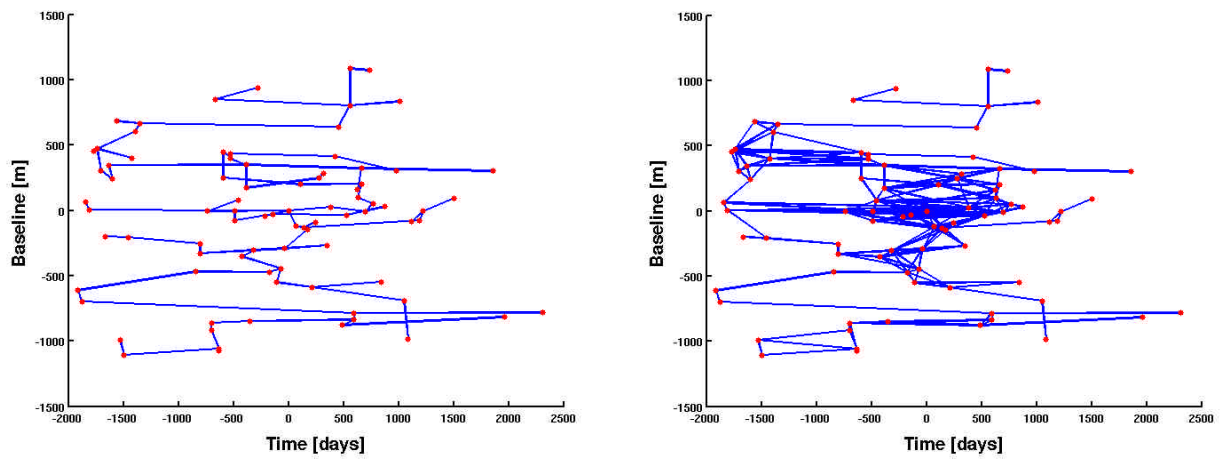
Figure 4 –Comparison between the MST (on the left) and the graph obtained by doubling the number of interferograms (on the right).
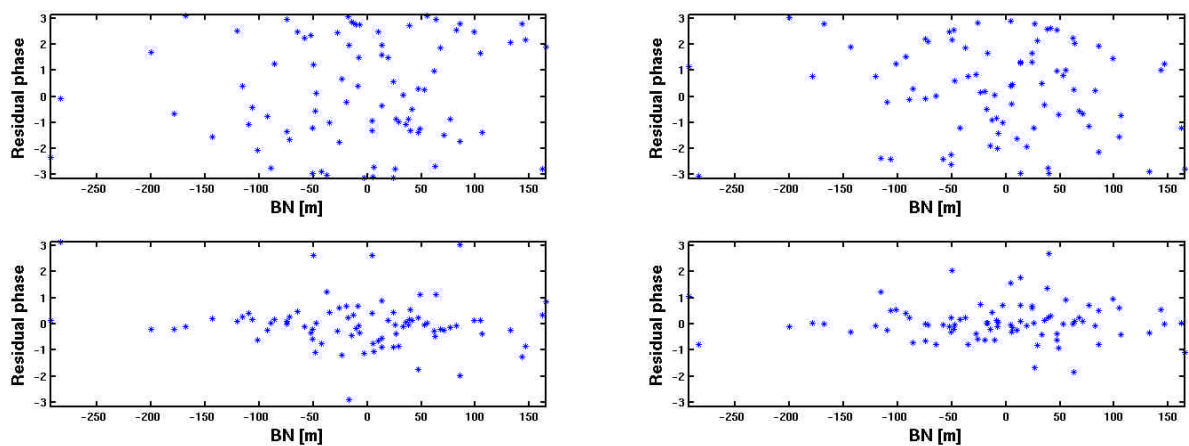
Figure 5 – Two examples (left and right) of phase residuals after compensating for the terms dependent on height and linear deformation trend. In the top images the phase is relative to a single pixel, in the bottom images the phase has been obtained by estimating the spatial coherence.
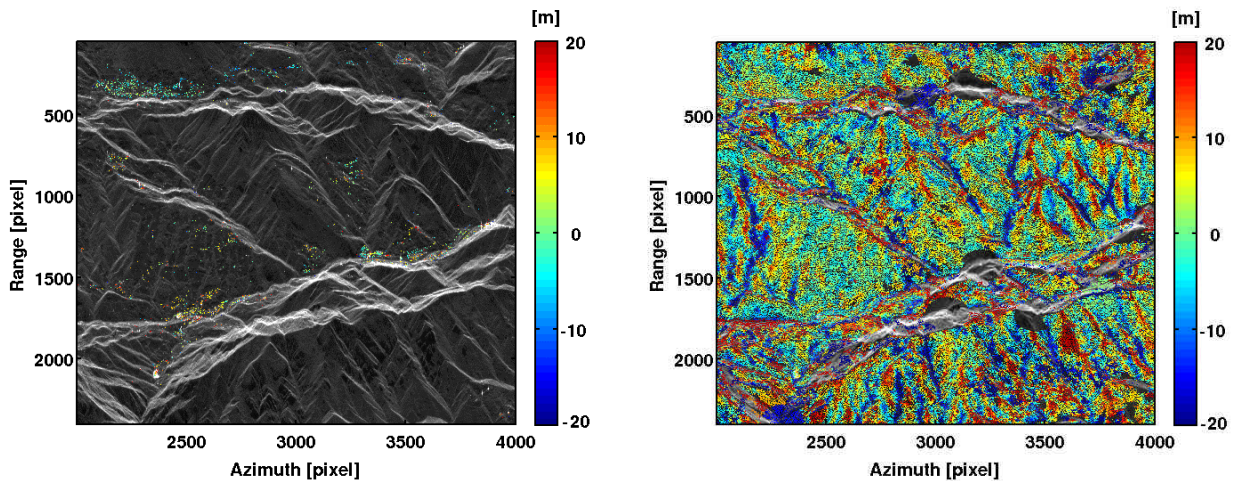
Figure 6 – Estimated residual height (with respect to SRTM data) in Dossena in a colour scale ranging 40m, for classical PS's (on the left) and for partially coherent targets (on the right).

RESULTS

The algorithm above described deals with the core processing step of the PS technique, namely the estimate of height and linear deformation trend of the targets. The algorithm can thus be easily inserted in the processing chain present in literature [2] without remarkable changes. We neglect here describing again the selection of PS Candidates (PSC), the generation of a spatial graph among PSC's and the estimate of the Atmospheric Phase Screen (APS). We introduce hence the analysed data-set and the significant results.

The processed area is partially visible as background in Figure 6 on the left. It corresponds to an area of approximately $400km^2$ on the ground. The data have been acquired by the European Space Agency (ESA) satellites ERS-1 and 2 from the descending Track 208, Frame 2673. The analysed 84 images cover the time-period from 1992 to 2003.

Figure 6 reports the first impressive result. The estimated residual height (with respect to SRTM data) is plotted in a colour scale ranging 40m for the classical PS's (on the left) and for the partially coherent targets detected with the proposed modifications (on the right). The two images are actually not fully comparable: the classical PS (~1500 points) have been selected posing a restrictive threshold on the temporal coherence (>0.7), whereas on the right 160.000 points have been chosen with a temporal coherence >0.4. Then, some errors due to the preliminary character of the work are visible in the picture on the right. Still, it is astonishing to appreciate the density of points even in vegetated areas and the height details that can be easily recognized. Moreover, it can be observed that most of the topographic features that have become visible are in correspondence of slope changes. This fact, that deserves future studies, can be at least firstly explained considering that SRTM errors lead not only to wrong height values in SAR coordinates, but to wrong height values also in wrong SAR coordinates. This shift between real and SRTM height data in SAR coordinates produces, when calculating their difference, a height step exactly in correspondence of slope changes.
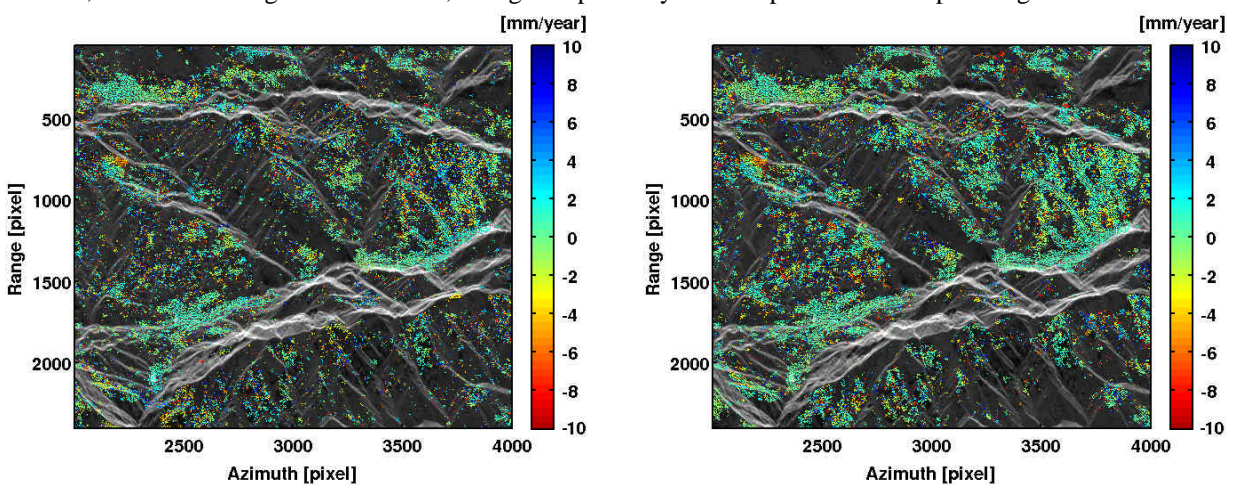
Figure 7 – Linear deformation trend of partially coherent targets in Dossena estimated with the MST (on the left) and by doubling the number of interferograms (on the right).
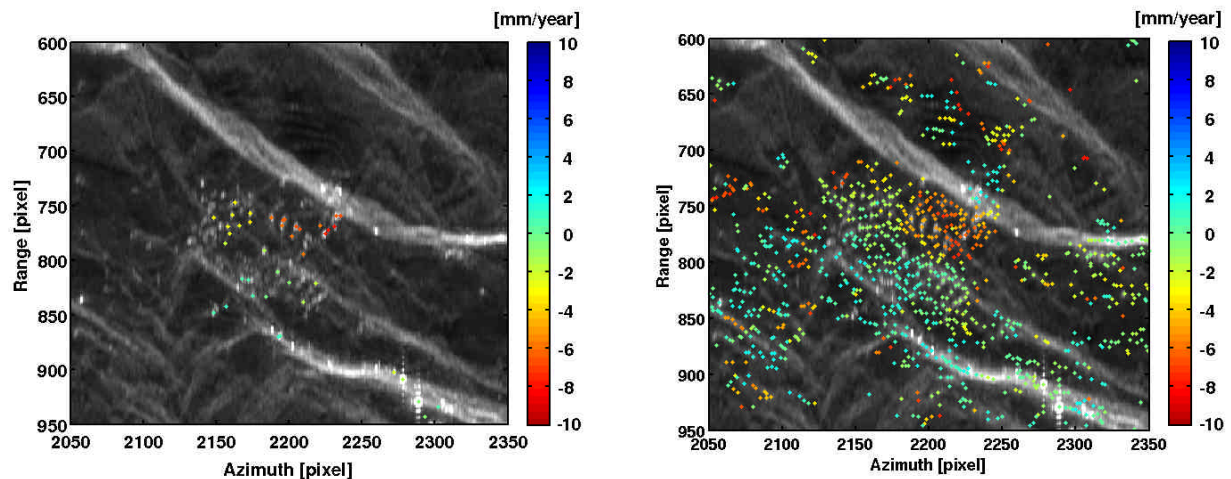
Figure 8 – Estimated linear deformation trends of PS's (on the left) and of partially coherent targets (on the right) around the municipality of Dossena. The orange-red identify the active landslide.

Figure 7 shows the results relative to the estimate of the linear deformation trend. The image on the left has been obtained by processing the Dossena site with the MST. The image on the right is the outcome of the addition of more interferograms to the minimum graph. In both cases, the visualized points have been selected by means of the temporal coherence (>0.4) and of the effective temporal baseline (>10). In the image on the right a slight higher density and a slight smaller variance of the deformation values can be observed.

Finally, in Figure 8 a comparison over the municipality of Dossena is depicted. On the left the PS and on the right the partially coherent targets velocities are shown. The deformation values of the two images are in good agreement. The main contribution of the novel technique resides in the precise identification of the moving area within the scene.

CONCLUSIONS

In this work the case study of Dossena, a small municipality in mountainous area in the province of Bergamo Italy, has been exploited to develop a new processing algorithm that allows to extract information also from partially coherent targets using spaceborne SAR data. Thus, very high densities of points can be reached also in extra-urban areas to monitor surface deformation phenomena and to retrieve Digital Elevation Maps. The results obtained in Dossena were exploited to precisely delimit the boundary of an active landslide on its territory.

ACKNOWLEDGEMENTS

REFERENCES

[1] Curlander J. C., McDonough R. N. (1991), "Synthetic Aperture Radar: Systems and Signal Processing", New York, John Wiley & Sons.

[2] Ferretti A., Prati C., Rocca F. (2001), "Permanent Scatterers in SAR Interferometry", *IEEE TGARS*, Vol. 39, no. 1.

[3] Dixon T.H., Amelung F., Ferretti A., Novali F., Rocca F., Dokkas R., Sella G., Kim S.W., Wdowinski S., Whitman D. (2006), "Subsidence and flooding in New Orleans", *Nature*, vol. 441, pp. 587-588.

[4] Ferretti A., Perissin D., Prati C., Rocca F., (2006) "On the physical characterization of SAR Permanent Scatterers in urban areas", *Proceedings of 6th European Conference on Synthetic Aperture Radar - EUSAR 2006*, Dresden (Germany), 16-18 May 2006.

[5] Ferretti A., Parizzi A., Perissin D., Prati C., Rocca F. (2006), "Accurate DEM reconstruction from Permanent Scatterers and multi-baseline interferometry", *Proceedings of the IEEE International Geoscience and Remote Sensing Symposium - IGARSS*, Denver (Colorado).

[6] Savio G., Ferretti A., Novali F., Musazzi S., Prati C., Rocca F. (2005) "PSInSAR Validation by means of a Blind Experiment Using Dihedral Reflectors" proceedings of FRINGE, Frascati, Italia.

[7] P. Berardino, G. Fornaro, R, Lanari, E. Sansosti, "A New Algorithm for Surface Deformation Monitoring based on Small Baseline Differential SAR interferograms", *IEEE TGARS*, vol. 40, no. 11, pp. 2375-2383, November 2002.

[8] Rocca F., "Modeling Interferogram Stacks", *IEEE TGARS*, vol. 45, no. 10, In Press.